THE JOURNAL OF PHYSICAL CHEMISTRY A

Article

pubs.acs.org/JPCA

Heterogeneous Reactions of Pirimiphos-Methyl and Pirimicarb with NO_3 Radicals

Youfeng Wang,[†] Bo Yang,*[,†] Peng Zhang,[†] Wang Zhang,[‡] Changgeng Liu,[†] Xi Shu,[†] and Jinian Shu[†]

[†]Research Center for Eco-Environmental Sciences, Chinese Academy of Sciences, Beijing 100085, China

[‡]Department of Environmental Engineering, Beijing General Research Institute of Milling and Metallurgy, Beijing 100160, China

Supporting Information

ABSTRACT: Pirimiphos-methyl (PMM) and pirimicarb (PM) are two typical *N,N*-dialkyl substituted pyrimidine pesticides. The heterogeneous reactions of suspended PMM and PM particles with NO_3 radicals are investigated using an online aerosol time-of-flight mass spectrometer and a real-time atmospheric gas analysis mass spectrometer. Three products for PMM and five products for PM are observed and assigned with the aid of GC/MS. Phosphoric acid 2-diethylamino-6-methyl-4-pyrimidinyl dimethyl ester and 2-(dimethylamino)-5,6-dimethyl-4-hydroxy-pyrimidine are the main reaction products observed for PMM and PM, respectively. The effective rate constants for the reactions of PMM and PM particles with NO_3 radicals are $(9.9 \pm 0.3) \times 10^{-12}$ and $(7.5 \pm 0.3) \times 10^{-13}$ cm^3 molecule^{-1} s^{-1}, respectively, obtained using a mixed-phase relative rate method. Geometries and energies of transition states (TS) and intermediates (IM) are obtained by DFT calculation to elucidate the detailed mechanism of the P═S group oxidation into the P═O group for PMM. The theoretical studies present the reasonable intermediates including the S-oxide and the diradical (IM1[a] and IM2[a]). The mechanism explanation may provide useful information for understanding the degradation mechanism of organothionophosphorus compounds in the environment.

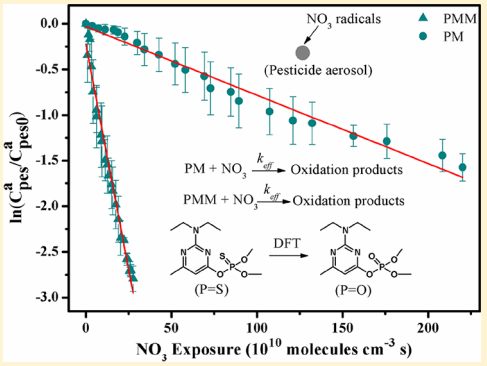

1. INTRODUCTION

Pesticides are toxic chemical substances widely used for pest control and weed killing. Considering their short- and long-range transports in the atmosphere,[1] pesticides contaminate the atmospheric environment severely and have potential harm to human health.[2] Most pesticides are semivolatile or low-volatile compounds that could exist in both gas and particulate phases in the atmosphere.[3−5] The atmospheric chemical transformations of pesticides mainly involve photolysis and the reactions with atmospheric oxidants (O_3, NO_x, and OH radicals).[6] The reaction products may be more toxic or carcinogenic than their precursors.[7]

Pirimiphos-methyl (PMM) and pirimicarb (PM) are two classical *N,N*-dialkyl substituted pyrimidine pesticides that are primarily used as acaricide and aphicide, respectively. They could exist in both gas and particulate phases in the ambient atmosphere according to their respective vapor pressures of 2.0×10^{-3} Pa (20 °C)[8] and 9.7×10^{-4} Pa (25 °C).[9] Chemical structures of PMM and PM are shown in Figure 1. Both of them have an *N,N*-dialkyl group adjacent to a pyrimidine ring, which is a common structure in insect repellents and industrial solvents owing to its important biological activity. Besides, PMM has a typical unsaturated phosphorus−sulfur double bond (P═S), and PM contains a carbamate group adjacent to the pyrimidine ring.

Many studies on transformations of PMM and PM in biosphere under various physical and biological conditions have been performed.[10−15] In 2002, Eneji et al. investigated the degradation of PMM in soil/water slurries and identified 2-diethylamine-4-hydroxy-6-methyl pyrimidine as the main product.[10] Chiron et al. reported three major degradation routes and five intermediate compounds in ozone treatment of PMM-containing industrial water.[11] In addition, 23 degradation products of PMM under titania photocatalysis in solution were identified by Herrmann et al.[12] The reported degradation pathways of PMM include hydrolysis of phosphoric ester function, *N*-dealkylation or formation of *N*-oxime, and the oxidation of methyl group into an aldehyde function.[10−12] The transformation of P═S into P═O observed in photocatalytic degradation of PMM is a common reaction for organothionophosphorus compounds, but the detailed reaction mechanism is not well-known. Recently, Yang et al. reported

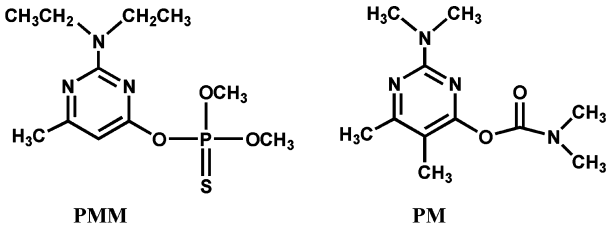

Figure 1. Chemical structures of PMM and PM.

Received: July 19, 2012
Revised: October 18, 2012
Published: October 19, 2012

the study on the heterogeneous reactivity of suspended PMM particles with ozone, and the obtained heterogeneous reactive rate constant of PMM particles toward gas phase ozone under room temperature (293 ± 2 K) was (1.97 ± 0.25) × 10^{-17} cm^3 $molecules^{-1}$ s^{-1}.[16]

The degradations of PM in water, soil, and organisms have also attracted attention. The carbamate-hydrolysis product (2-dimethylamino-5,6-dimethyl-4-hydroxypyrimidine) and its subsequent *N*-demethylation products (2-methylamino-5,6-dimethyl-4-hydroxypyrimidine and 2-amino-5,6-dimethyl-4-hydroxypyrimidine) were identified as the major metabolites of PM in human urine.[13] The carbamate-hydrolysis product and carbamate-containing products (*N*-demethylation and carbonylation of the *N*,*N*-dimethy group, i.e., 2-[(methylformyl)-amino]-5,6-dimethylpyrimidin-4-yl dimethylcarbamate and 2-(methylamino)-5,6-dimethylpyrimidin-4-yl dimethylcarbamate) were identified as the photodegradation products in aqueous environments.[14,15] Therein, The carbamate-hydrolysis product was the major microbial degradation product of PM in soil.[14] The carbamate-containing products were observed as the photodegradation products of PM in soil.[15]

NO_3 radicals are an important nighttime oxidant in the troposphere and influence the degradation pathways and lifetimes of many atmospheric organics. However, to our knowledge, the heterogeneous reactions of PMM and PM particles with NO_3 radicals have not been reported yet. In this study, the heterogeneous reactions of suspended PMM and PM particles with NO_3 radicals are investigated. The reactions are performed in an aerosol reaction chamber coupled with an online vacuum ultraviolet photoionization aerosol time-of-flight mass spectrometer (VUV-ATOFMS) and an online atmospheric gas analysis mass spectrometer. Off-line GC/MS analyses are also conducted for product identification. The effective rate constants are measured via the relative rate method. The reaction pathways are proposed. In addition, the quantum chemistry methods are employed to explore the detailed mechanism for the oxidation of P═S into P═O.

2. EXPERIMENTAL METHODS

2.1. Experimental Setup. The experimental setup has been described in detail elsewhere.[17] In short, it consists of an aerosol generator, a reaction chamber, and online analytical instruments.

The aerosol generator is an electric tubular oven comprising two tandem quartz tubes, each of which is 40 cm (length) × 3 cm (outer diameter) and equipped with a temperature controller. The suspended particles are generated by the homogeneous nucleation method. Azelaic acid (0.1 g) in the first tube is used to generate nuclei through high temperature gasification and then condensation. Azelaic acid is inert toward NO_3 radicals. No apparent reaction product is observed with ATOFMS for pure azelaic acid particles exposed to NO_3 radicals (~5 × 10^9 molecules cm^{-3}) for 10 min. Another 0.1 g of pesticide sample is placed in the second tube. It is gasified and coated on the azelaic acid nuclei. The N_2 flows through the two quartz tubes sequentially at 0.6 L min^{-1} to introduce the generated pesticide particles into the reaction chamber, which are monitored with a scanning mobility particle sizer (SMPS, TSI 3080). The coating thicknesses of the suspended pesticide particles are controlled by adjusting the temperature of the quartz tubes and the flow rate of N_2. The temperature of the two tubes for generating suspended PMM particles are set at 418 ± 1 and 388 ± 1 K, respectively, while those for PM particles are at 413 ± 1 and 393 ± 1 K. The particles generated in the experiments are polydispersed: the geometric mean diameters of PMM particles and their nuclei are 245 and 204 nm, and those for PM particles and their nuclei are 297 and 257 nm. The corresponding geometric standard deviations of the particle size distributions are 1.86 and 1.44, respectively, for PMM and PM particles.

The reaction chamber consists of a ~180 L thin-walled open head stainless steel drum and a collapsible Teflon bag.[17] Before each experiment, the reactor is rinsed with ethanol, dried in hot air, and filled with the filtered air. The experiments are conducted under atmospheric pressure and room temperature (~298 K). The relative humidity in the chamber is roughly estimated to be 10% due to the residual filtered air in the chamber. The initial mass concentrations for PMM and PM particles in the chamber are 471 ± 17 and 208 ± 15 μg m^{-3} respectively. Isoprene is injected into the chamber as the reference compound. The concentration of isoprene is monitored with an online atmospheric gas analysis mass spectrometer (QIC-20-HAL3F-RC, Hiden) via detection of the mass peak at m/z 67 ($C_5H_7^+$). The initial concentration of isoprene in the chamber is ~4 × 10^{14} molecules cm^{-3}. When its concentration stabilizes, a N_2 flow at the rate of 0.6 L min^{-1} passes through a flask that contains N_2O_5 powder placed at the room temperature and introduces gaseous N_2O_5 continuously into the chamber during the reaction. A stainless steel fan at the bottom keeps rotating during the reactions, driven by a magnetic stirring apparatus outside the chamber.

Pesticide particles and their reaction products are analyzed in real time with a laboratory-built VUV-ATOFMS.[18] An 8 mm diameter copper rod coupled with a cartridge heater placed in the detection chamber is used to vaporize the particles, and the nascent organic vapor is photoionized with light radiated from a home-assembled VUV lamp powered by RF of 80 W. The VUV irradiation is achieved by exciting a 180 Pa mixture of 5% krypton in helium (v/v) with a copper coil driven by a 13.56 MHz RF power supply and outputs ~5 × 10^{14} photons s^{-1}.

Four duplicate experiments are performed for the heterogeneous reaction of each pesticide. One experiment is conducted to observe reaction products preferably, and the atmospheric gas analysis mass spectrometer and VUV-ATOFMS, respectively, monitor the concentrations of isoprene and pesticide particles every 22 s. The data of the other three duplicate experiments are recorded every 12 s for kinetic study of the heterogeneous reactions. Since the concentration of pesticide particles is linear with the signal intensity of the mass peak measured by ATOFMS,[18] the decay rate of signal intensity is equal to that of pesticide concentration.

2.2. NO_3 Radical Preparation. NO_3 radicals are generated by thermal decomposition of N_2O_5 synthesized by dehydrating concentrated nitric acid with P_2O_5 powder.[19] The N_2O_5 collected is white powder contained in a 1000 mL flask and kept in a liquid nitrogen Dewar before use. During the experiment, the N_2O_5 powder vaporizes into gaseous N_2O_5 and then decomposes into NO_2 and NO_3 radical in the reaction chamber at room temperature.[20] The calculated concentrations of the NO_3 radicals in the chamber for these experiments are (0.6–7.0) × 10^9 molecules cm^{-3} according to the measured decay rates of isoprene ((0.4–1.9) × 10^{-3} s^{-1}) and the reported rate constant of the reaction between isoprene and NO_3 radical (7 × 10^{-13} cm^3 $molecule^{-1}$ s^{-1}) at 298 K.[21]

2.3. GC/MS Analyses. GC/MS analyses are conducted to help to identify the reaction products. Ten milligrams of pure

dx.doi.org/10.1021/jp3071635 | J. Phys. Chem. A 2012, 116, 10802–10809

pesticide is placed in the conical flask. A N_2 flow at 0.6 L min^{-1} introduces gaseous N_2O_5 continuously into the conical flask for ~15 min. After the reaction, 100 mL of CH_2Cl_2 is added into the conical flask and then ultrasonic-washed for ~5 min. One part of the solution is atomized into suspended droplets and analyzed directly with VUV-ATOFMS. In this experiment, the TOF mass spectra of the products from the reaction in the conical flask are similar to those from the particulate reaction in the chamber. Meanwhile, another part of the solution is analyzed with GC/MS for product identification.

The GC/MS (Agilent 6890) is equipped with a 30 m × 0.25 mm × 0.25 μm HP-5 capillary and an HP-5973 quadrupole mass filter with a 70 eV electron impact ionizer. The temperature of the capillary column is programmed from 60 to 130 °C at 23 °C min^{-1} and from 130 to 210 °C at 10 °C min^{-1}, up to 280 °C at 5 °C min^{-1}. One microliter of sample is injected via the pulsed splitless mode. The products are analyzed by GC/MS in the total ion chromatogram (TIC) mode and identified by comparing the EI mass spectra with the data from NIST Mass Spectral Library 2005.

2.4. Chemicals. PMM (Dikma, 99.5%), PM (Dikma, 99.5%), azelaic acid (NRSCRD, China, 99%), isoprene (99%, Alfa Aesar), fuming nitric acid (Beijing Lisui Chemical Factory, 95%), P_2O_5 (Sinopharm Chemical Reagent Co., Ltd., 98%), absolute ethyl alcohol (Sinopharm Chemical Reagent Co., Ltd., 99.7%), and dichloromethane (J. T. Baker Co., chromatographic grade) are used in the experiment. Nitrogen (99.99%) is purchased from Beijing Huayuan Gas Chemical Industry Co., Ltd.

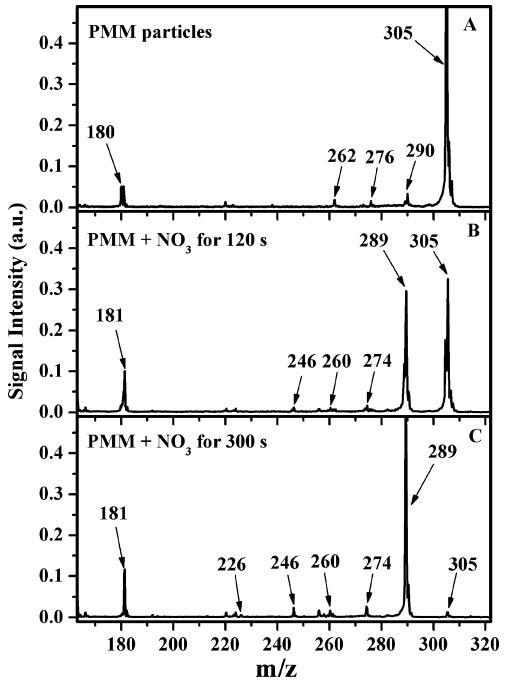

Figure 2. VUV-ATOFMS spectra of PMM particles (A) and its products in the reaction with NO_3 radicals for 120 (B) and 300 s (C). The acquisition time for each mass spectrum is 20 s and the peak intensity of each spectrum is normalized to the highest peak at m/z 305 shown in Plot A.

3. COMPUTATIONAL METHODS

All calculations are performed using the Gaussian09 program package.[22] Geometry optimization and frequency analysis are conducted using density functional theory (DFT) at the B3LYP/6-31G(d) level. The transition states (TS) are verified by intrinsic reaction coordinate (IRC) calculations to connect the desired intermediates (IM). In order to obtain more reliable relative energies of each stationary point on the potential energy surfaces, a single-point energy calculation has been performed on the 6-311++G(d,p) basis set and corrected with zero-point vibrational energies from the B3LYP/6-31G(d) level.

4. RESULTS AND DISCUSSION

The maximum average concentrations of NO_2 and N_2O_5 in this work are estimated to be 6.0×10^{13} and 6.8×10^{12} molecules cm^{-3}, respectively, according to the loss of isoprene and the thermal decomposition rate of N_2O_5 at ~298 K.[23] The reactivities of PMM and PM toward NO_2 are verified by exposing the pesticide particles to NO_2 with a concentration of 2.5×10^{14} molecules cm^{-3} for 10 min. There is no product mass peak observed with ATOFMS. Since the reaction time of the pesticide particles with NO_3 radicals is less than 10 min, the influence of direct reaction between NO_2 and the pesticide particles is neglected in this study. Since the reactive uptake coefficients of NO_3 radicals on most organic substance surfaces were 3−4 orders of magnitude higher than those of NO_2 and N_2O_5,[24−26] the effects of N_2O_5 on the loss of pesticide are also ignored in the experiment.

4.1. Reaction Products of PMM Aerosols. The TOF mass spectra of PMM ($C_{11}H_{20}N_3O_3PS$, MW = 305 g mol^{-1}) particles and their oxidation products shown in Figure 2A−C are acquired at 0, 120, and 300 s interaction time of the particles with NO_3 radicals. The intensities of mass peaks shown in Figure 2 are normalized to the intensity of the mass peak at m/z 305 shown in Figure 2A, which arises from the molecular ion of PMM. The weaker mass peaks at m/z 180, 262, 276, and 290 are the daughter ion mass peaks of PMM. As shown in Figure 2, the mass peak of the molecular ion of PMM (m/z 305) decreases gradually after exposure to NO_3 radicals. Meanwhile, two new peaks at m/z 181 and 289 appear and rise with the reaction time. These new mass peaks are contributed from the reaction products of PMM particles. Other three mass peaks at m/z 246, 260, and 274 are tentatively assigned as daughter ion peaks of the main product (m/z 289) since their profiles are similar to that of the daughter ion peaks of PMM. A small mass peak at m/z 226 appears in the later stage of the reaction, which is assigned to the secondary product of the reaction. The EI mass spectra of the three reaction products are obtained by GC/MS analyses, but the corresponding standard EI mass spectra are not available. Thus, we assign the products based on the molecular ions from VUV-ATOFMS, the EI mass spectra from GC/MS, and reported degradation products of the pesticides. Assignments for the reaction products of PMM are listed in Table 1.

Product I[a] (m/z 289) is assigned to phosphoric acid 2-(diethylamino)-6-methyl-4-pyrimidinyl dimethyl ester ($C_{11}H_{20}N_3O_4P$, MW = 289 g mol^{-1}), and Product II[a] (m/z at 181) is 2-diethylamine-4-hydroxy-6-methyl pyrimidine ($C_9H_{15}N_3O$, MW = 181 g mol^{-1}). The main ions and relative abundances of both the products obtained with GC/MS in EI modes show good consistency with the experimental results of Herrmann et al.[12] Since the benzene ring is the active sites of the nitro substitution reaction,[19,27] we speculate that the pyrimidine ring is more active than the functional groups in the

dx.doi.org/10.1021/jp3071635 | J. Phys. Chem. A 2012, 116, 10802−10809

Table 1. Reaction Products of PMM and PM with NO_3 Radicals Identified Based on the Molecular Ion Peaks from VUV-ATOFMS, the Results of GC/MS Analysis, and Reported Degradation Products[a]

Compound	*m/z*	RT	*η*	ref
PMM	305	13.7		NIST
Product I[a]	289	13.2	0.736	12
Product II[a]	181	8.8	0.245	12
Product III[a]	226	12.0	0.019	
PM	238	12.5		NIST
Product I[b]	167	9.4	0.891	13,15
Product II[b]	224	12.7	0.035	NIST[15]
Product III[b]	153		0.035	15
Product IV[b]	212	14.4	0.014	
Product V[b]	252		0.024	15

[a] *m/z* stands for the molecular ion peaks obtained with VUV-ATOFMS, RT is the retention time (min) of the product observed by GC/MS, and *η* represents the relative intensity of the molecular ion peaks obtained with VUV-ATOFMS. Ref is the reference reporting the degradation product (NIST represents that the compound is identified by a similar search using NIST library).

nitro substitution reaction. Thus, Product III[a] is assigned as 2-diethylamine-4-hydroxy-5-nitro-6-methyl pyrimidine ($C_9H_{14}N_4O_3$, MW = 226 g mol^{-1}), considering that the mass spacing between Products II[a] and III[a] is 45 amu, indicating one nitro group (NO_2, MW = 46 g mol^{-1}) added and one hydrogen atom (H, MW = 1 g mol^{-1}) removed at the substitution position.

4.2. Reaction Products of PM Aerosols. Figure 3A shows the TOF mass spectrum of PM ($C_{11}H_{18}N_4O_2$, MW = 238 g mol^{-1}) particles before exposure to NO_3 radicals. The mass peaks at *m/z* 238, 193, and 166 correspond to the molecular ion and two fragment ions of PM, respectively. Mass spectra shown in Figure 3B,C are acquired 130 and 320 s after the injection of N_2O_5 into the chamber. Compared to the mass spectrum shown in Figure 3A, there are two new mass peaks appearing at *m/z* 167 and 224, both of which are also observed in GC/MS analyses. Several new mass peaks with very weak intensities appear at *m/z* 153, 212, and 252 (shown in the inset of Figure 3C), while only the one at *m/z* 212 is detected by GC/MS. These inconsistencies may result from the different detection limits of two analytical instruments and the thermal instability and chemical polarity of chemicals.

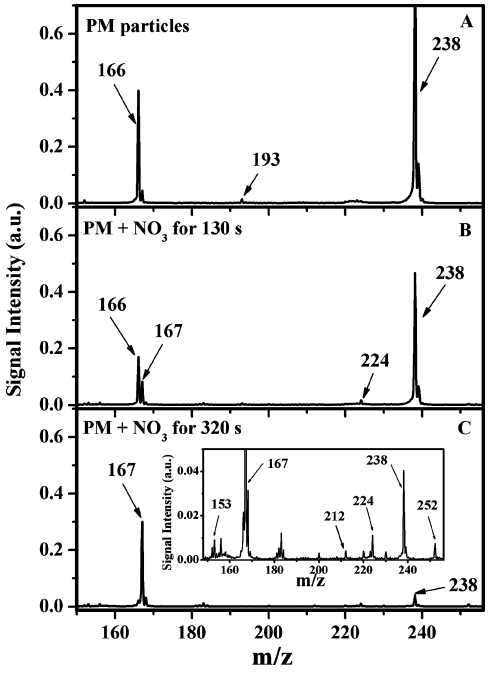

Figure 3. VUV-ATOFMS spectra of PM particles (A) and its products in the reaction with NO_3 radicals for 130 (B) and 320 s (C). The acquisition time for each mass spectrum is 20 s and the peak intensity of each spectrum is normalized to the highest peak at *m/z* 238 shown in Plot A.

Table 1 lists the assignments for the reaction products of PM. The mass peak at *m/z* 167 is assigned to 2-(dimethylamino)-5,6-dimethyl-4-hydroxy-pyrimidine (Product I[b], $C_8H_{13}N_3O$, MW = 167 g mol^{-1}), which is one of the major urinary metabolites in mammals by hydrolysis of the carbamate moiety.[13] The mass peak at *m/z* 224 is identified as 2-(methylamino)-5,6-dimethylpyrimidin-4-yl dimethylcarbamate (Product II[b], $C_{10}H_{16}N_4O_2$, MW = 224 g mol^{-1}) using the NIST library, which is formed by *N*-dealkylation of one methyl adjacent to the N atom connected to the pyrimidine ring. The mass peak at *m/z* 153 is assigned to the molecular ion peak of 2-(methylamino)-5,6-dimethyl-4-hydroxy-pirimidine (Product III[b], $C_7H_{11}N_3O$, MW = 153 g mol^{-1}), which is considered as the secondary product of Product II[b] because the signal intensity of Product II[b] grows first and then reduces, while that of Product III[b] grows slowly all the way to the maximum. Considering the mass space between *m/z* 167 and 212, we speculate that the mass peak at *m/z* 212 results from the nitro-substitution of Product I[b]. Thus, the mass peak at *m/z* 212 is tentatively assigned to the molecular ion of 2-(dimethylamino)-5,6-dimethyl-4-nitrooxy-pyrimidine (Product IV[b], $C_8H_{13}N_4O_3$, MW = 212 g mol^{-1}). The conversion between Product I[b] and IV[b] may be reversible since nitroxy-substituents on the radical carbon are unstable, dissociating by O−N bond scission leading to a carbonyl compound and NO_2.[28] The mass peak at *m/z* 252 is assigned as 2-[(methylformyl)amino]-5,6-dimethylpyrimidin-4-yl dimethylcarbamate (Product V[b], $C_{11}H_{16}N_4O_3$, MW = 252 g mol^{-1}) by formation of the carbonyl group on the *N,N*-dimethyl group, which is one of the main photoproducts of PM in water solution and solid phase.[15] The mass peaks at *m/z* 156, 183, and 200, which may be originated from fragments of products or impurities of pesticide samples, cannot be assigned.

Though both studied pesticides contain *N,N*-dialkyl substituted structures (*N,N*-diethyl for PMM and *N,N*-dimethyl for PM), the reactivities of the two groups toward NO_3 radicals are different. The *N,N*-diethyl group of PMM does not react with NO_3 radicals, while the *N,N*-dimethyl group of PM undergoes the *N*-dealkylation and the carbonylation reactions in the experimental conditions. This result may indicate that the *N,N*-diethyl group is more stable than the *N,N*-dimethyl group adjacent to the pyrimidine ring.

4.3. Effective Rate Constants for the Pesticide Particles with NO_3 Radicals. The effective rate constants (k_{eff}) for the reactions of PMM and PM particles with NO_3 radicals are obtained by the mixed-phase relative rate method[29] with isoprene as the reference compound. The expression of the relative kinetics can be presented by eq 1.[30]

$$\ln(C^a_{pes}/C^a_{pes0}) = (k^a_{pes})\left[\frac{\ln(C^g_{ref}/C^g_{ref0})}{k^g_{ref}}\right] \quad (1)$$

dx.doi.org/10.1021/jp3071635 | J. Phys. Chem. A 2012, 116, 10802−10809

where C^a_{pes} and C^g_{ref} are the respective concentrations of aerosol-phase pesticide and gas-phase reference species (molecules cm^{-3}), C^a_{pes0} and C^g_{ref0} are the respective initial concentrations of pesticide particles and gas-phase reference compound in the reaction chamber (molecules cm^{-3}), k^a_{pes} represents the corresponding effective particle-phase reaction rate constant (cm^3 $molecule^{-1}$ s^{-1}), k^g_{ref} is the reaction rate constant of the gas-phase reference species (7.0×10^{-13} cm^3 $molecule^{-1}$ s^{-1} at 298 K);[21] whereas $(\ln(C^g_{ref}/C^g_{ref0}))/(-k^g_{ref}) = \int_0^t C^g_{NO_3} dt = \overline{C^g_{NO_3}}t$, eq 1 can be represented as eq 2.

$$\ln(C^a_{pes}/C^a_{pes0}) = -k^a_{pes}\,\overline{C^g_{NO_3}}\,t \quad (2)$$

Here, $C^g_{NO_3}$ and $\overline{C^g_{NO_3}}$ are the time-dependent and averaged concentrations of NO_3 radicals in the gas phase (molecules cm^{-3}) respectively. Therefore, the effective rate constants of particles can be obtained by measuring the decay rates of particles and the gas-phase reference compound concurrently in the mixed-phase reaction.

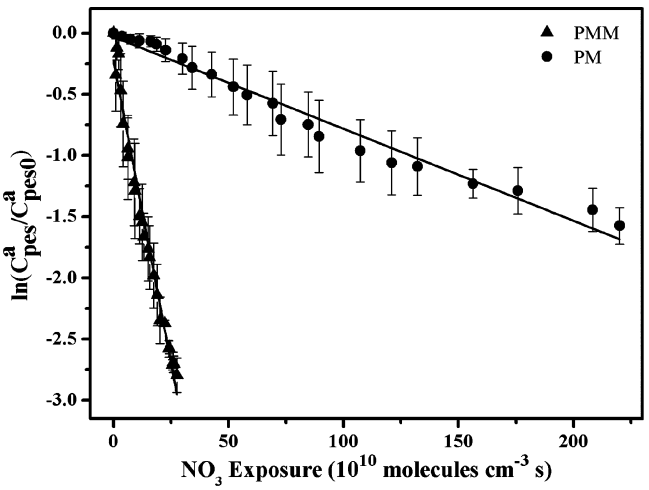

Figure 4. Plots of $\ln(C^a_{pes}/C^a_{pes0})$ versus NO_3 exposure ($\overline{C^g_{NO_3}}t$) for the reactions of NO_3 radicals with PMM and PM particles.

Figure 4 shows the plots of the measured $\ln(C^a_{pes}/C^a_{pes0})$ as the function of NO_3 exposure ($\overline{C^g_{NO_3}}t$) for the two pesticides. Error bars represent the standard deviations of the three duplicate experiments. The wall losses (<5%) of the two pesticide particles are ignored in the data processing. The data points are well fitted with a linear equation ($R^2 > 0.97$). According to eq 3, the slopes of the fit lines represent the effective rate constants of the pesticide particles. Thereby, the effective rate constants (k_{eff}) $(9.32 \pm 0.32) \times 10^{-12}$ and $(7.51 \pm 0.27) \times 10^{-13}$ cm^3 $molecule^{-1}$ s^{-1} are obtained for PMM and PM aerosols, respectively. It is obvious that the reactivity of PMM toward NO_3 radicals is higher than that of PM. The homogeneous reaction rate constants of the similar organic phosphorus compounds ($(C_2H_5O)_2P(S)CH_3$ and $(C_2H_5O)_3PS$) with OH radicals, NO_3 radicals, and O_3 are on the order of 10^{-10}–10^{-11}, 10^{-15}, and $<6 \times 10^{-20}$ cm^3 $molecule^{-1}$ s^{-1}, respectively.[31] It is speculated that the homogeneous reaction rate constant of PMM with NO_3 radicals are probably ~3 orders of magnitude slower than the heterogeneous rate constant.

Because of the volatilization of the pesticide particles, there would be a certain amount of gas phase pesticide in the chamber. Before introducing N_2O_5 into the reaction chamber, the size distribution and the number concentration of pesticide particles reach stable, indicating a partitioning equilibrium between the particle phase and gas phase pesticide in the chamber. The initial gas/particle distribution ratios in our experiments are calculated to be ~1/2 for the two pesticides (The detailed calculation is described in Supporting Information). The gas-particle partitioning may influence the kinetic measurements at a certain extent during the reaction by two ways: volatilization from the particle surface to the gas phase and condensation from the gas phase to the particle phase. Considering that the homogeneous reaction rates are always lower than the heterogeneous reaction rates for the same reactants[24,32−34] and that the absorbed gas-phase reactants and reaction products on the surfaces of particles may inhibit the volatilization of the pesticides during the reaction, we speculate that the condensation of pesticide from gas phase to the particle phase would predominate the repartitioning process caused by reaction and that the measured reaction rate constants may be underestimated.

4.4. Uptake Coefficients. The uptake coefficient is defined as the fraction of the collisions between a gas molecule and a particle that result in reaction. The uptake coefficients (γ) of NO_3 radicals on PMM and PM particles are calculated using eq 3 according to a spherical shell model.[30]

$$\gamma = \frac{(R_p^3 - R_c^3)\rho_{pes} N_A \eta_{pes}}{3 M_{pes} R_p D_g \overline{C^g_{NO_3}}\,t} \quad (3)$$

where R_p and R_c are the respective particle radius and inner core radius (cm), ρ_{pes} the pesticide density (1.2 g cm^{-3} for PMM and 1.1 g cm^{-3} for PM), N_A the Avogadro's number, η_{pes} the ratio of consumption (~0.9 and 0.75 for PMM and PM, respectively, in our experiments), M_{pes} the pesticide molecular weight (g mol^{-1}), D_g diffusion coefficient (~1 cm^2 s^{-1}) for NO_3 radicals,[30] and t the reaction time (s).

The uptake coefficients for NO_3 radicals on PMM and PM particles are 0.15 and 0.05, respectively, indicating that 15% and 5% of the NO_3 collisions with PMM and PMM yield reactions. Since the model is based on the consumption of particulate pesticide, the pesticide loss induced by reactive intermediates and evaporation followed by oxidation might influence the uptake coefficients. However, these influences are hard to quantify under the experimental conditions. The calculated uptake coefficients for NO_3 radicals on PMM and PM particles are close to those of NO_3 radicals on PAH particles.[30]

The atmospheric lifetimes of the PMM and PM particles at the lower tropospheric concentration of NO_3 radicals at night (5×10^8 molecules cm^{-3})[35,36] are calculated to be ~6 and 21 days, respectively (the detailed calculation is presented in the Supporting Information). However, the real atmospheric lifetimes of the two pesticide particles may vary greatly due to the different concentrations of oxidants, different aerosol surface-area-to-volume ratios, or different gas-particle phase partitioning under real atmospheric conditions.

4.5. Reaction Pathway. Figure 5A shows the reaction pathways of PMM particles with NO_3 radicals. It has two reaction pathways. One is the transformation of P═S into P═O. It initiates by the addition of oxygen to the sulfur atom, giving the intermediate IM1[a]. The rearrangement intermediate IM2[a] is a diradical and then yields Product I[a] via the subsequent

dx.doi.org/10.1021/jp3071635 | J. Phys. Chem. A 2012, 116, 10802−10809

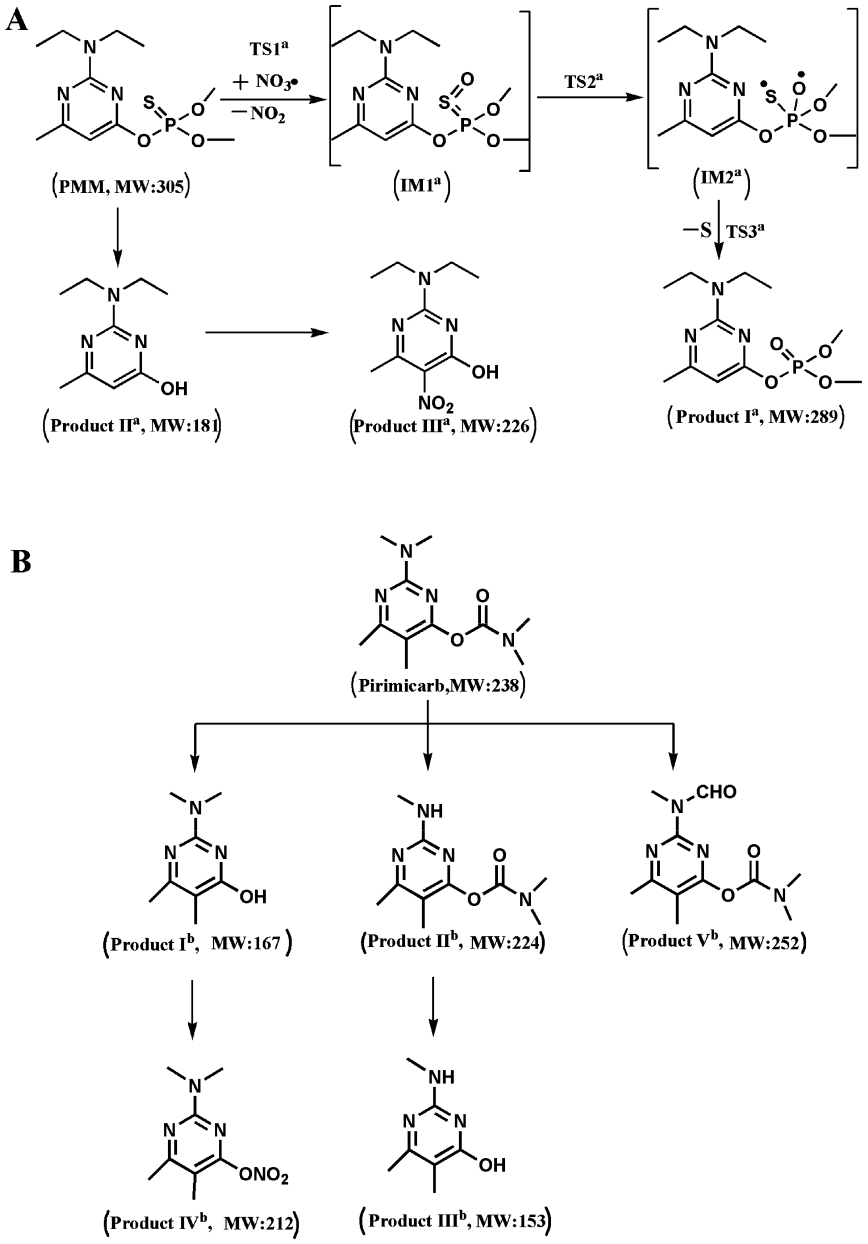

Figure 5. Proposed pathways for the reactions of NO_3 radicals with PMM particles (A) and PM particles (B).

loss of a sulfur atom with retention of configuration of the phosphorus atom. Another pathway is the breakage of the O−P bond under the attack of NO_3 radicals and following abstraction of an H atom, leading to the formation of Product II^a. Then, Product II^a can be converted into Product III^a via further reaction with the NO_3 radicals of which the formation mechanism may be similar to that of naphthalene with NO_3 radicals.[37] Figure 5B shows the three pathways for the reaction of PM particles with NO_3 radicals. The first pathway is the transformation of the carbamate group into a hydroxyl group resulting in the formation of Product I^a. Then, the nitration of Product I^b yields Product IV^b. The second pathway involves the formation of the *N*-dealkylation product, Product II^b. It can convert into Product III^b through secondary reaction. The third pathway is the oxidation of the α-carbon of *N*,*N*-dimethyl to form a carbonyl group. There are some discrepancies between the proposed pathways in this study and those of PM photolysis in water and solid phases,[15] which may be due to the differences of degradation circumstances.

4.6. Oxidation Mechanism of the P═S Group. The energy profile for transformation of the P═S into the P═O group in the reaction between PMM and NO_3 radicals is illustrated in Figure 6. The related optimized geometries of the TS and IM are depicted in Figure S1, Supporting Information. It initiates directly by transfer of an oxygen atom from the NO_3 radical to an unbounded electron pair on the sulfur atom, as shown in $TS1^a$. With only one imaginary frequency at 695.24i cm^{-1}, the $TS1^a$ shows a vibration in which the O atom interchanges position between the sulfur (S) and nitrogen (N) atoms. The phosphorus−sulfur bond length in $TS1^a$ (2.011 Å) is an intermediate value between the P−S bond in $IM1^a$ (2.116 Å) and the P═S double bond within PMM (1.937 Å), consistent with delocalization of π-electron density into this bond. The reaction coordinate from $TS1^a$ to $IM1^a$ by removal of the gaseous nitrogen dioxide can be described in terms of an

dx.doi.org/10.1021/jp3071635 | J. Phys. Chem. A 2012, 116, 10802−10809

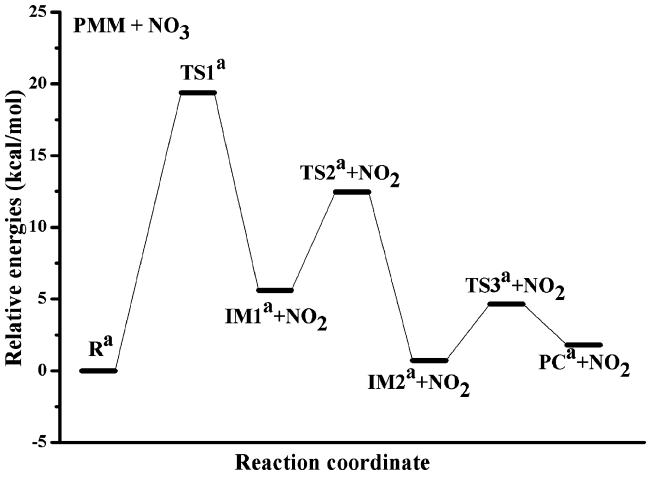

Figure 6. Energy profile of the reaction pathway leading to the formation of Product I[a] at the level of B3LYP/6-311++G(d,p)//B3LYP/6-31G(d) theory. R, reactant; TS, transition state; IM, intermediate; PC, product complex. All values are in kcal mol^{-1} relative to the reactants.

enlargement of the P−S bond (2.116 Å), the P−S−O[1] bond angle (105.867°), and the formation of the sulfur−oxygen bond (1.556 Å).

The TS2[a] shows an imaginary frequency of 234.37i cm^{-1} with the change of angle P−S−O[1] and the bond lengths of P−S and S−O[1]. Also, the imaginary frequency of TS3[a] is 61.18i cm^{-1}, involving a slight change of P−S and P−O[1] bond lengths.

Table 2 illustrates the energy, enthalpy, and free energy of various species relative to the reactants for the formation pathway of Product I[a]. There is great possibility for these reactions to go spontaneously in the atmosphere because all the activation energy barriers are less than 20 kcal mol^{-1} (Figure 6). The relative energy of PC[a] + NO_2 is 1.798 kcal mol^{-1}, while that of Product I[a] + sulfur + NO_2 is 35.139 kcal mol^{-1}. Therefore, we speculate that there is little possibility for the sulfur to be released spontaneously as an elementary substance since the energy barrier would be more than 30 kcal mol^{-1}. In the enzymatic reaction of parathion, most of the sulfur released becomes covalently bound to macromolecules,[38] but the fate of sulfur in the model reaction is unknown. The transformation of P═S into the P═O group is very common for organothionophosphorus compounds, whatever in water, soil, and atmospheric environments; these initial theoretical results may help to understand the transformation mechanism of the P═S group in the environment.

Table 2. Relative Energies (*E*, in kcal mol^{-1}), Relative Enthalpies (*H*, in kcal mol^{-1}), and Relative Free Energies (*G*, in kcal mol^{-1}) of Related Species for the Formation of Product I[a]

Species	*E*	*H*	*G*
R[a]	0	0	0
TS1[a]	19.382	22.443	32.016
IM1[a] + NO_2	5.617	10.257	10.722
TS2[a] + NO_2	12.457	14.704	16.026
IM2[a] + NO_2	0.719	−2.187	−0.882
TS3[a] + NO_2	4.636	1.219	3.344
PC[a] + NO_2	1.798	−0.194	0.532

4. CONCLUSIONS

Heterogeneous reactions of NO_3 radicals with suspended PMM and PM particles are investigated. The main reaction products for PMM and PM particles are obtained, and the degradation pathways are proposed. The effective rate constants of PMM and PM particles with NO_3 radicals are obtained using the mixed-phase relative rate method. The experimental results reveal that NO_3 radicals have high reactivity toward PMM and PM particles and should influence remarkably the degradation pathways of PMM and PM particles during nighttime. DFT studies present the reasonable intermediates (IM1[a] and IM2[a]) in the transformation of P═S into P═O, for which the reaction mechanism for years has not been well-known. PMM and PM are the representatives of the *N*,*N*-dialkyl substituted pyrimidine pesticides. These experimental and theoretical studies on their reactions with NO_3 radicals are significant for understanding atmospheric transformation of the two pesticides and their analogues.

■ ASSOCIATED CONTENT

Supporting Information

Additional 3 equations and one figure with information on initial gas/particle distribution ratios, the atmospheric lifetimes, and the geometrical structures of the B3LYP/6-31G(d) optimized stationary points for the reaction pathway of Product I[a]. This material is available free of charge via the Internet at http://pubs.acs.org.

■ AUTHOR INFORMATION

Corresponding Author

*Tel: +86 10 62849087. Fax: +86 10 62923563. E-mail: boyang@rcees.ac.cn.

Notes

The authors declare no competing financial interest.

■ ACKNOWLEDGMENTS

This work is funded by National Natural Science Foundation of China (Grant No. 21077115) and Creative Research Groups of China (Grant No. 50921064).

■ REFERENCES

(1) Sanusi, A.; Millet, M.; Mirabel, P.; Wortham, H. *Sci. Total Environ.* **2000**, *263*, 263−277.

(2) Dinham, B. *The Pesticide Hazard: A Global Health and Environmental Audit*; Zed Books Ltd. in association with The Pesticides Trust: London, 1993.

(3) Sauret, N.; Wortham, H.; Putaud, J. P.; Mirabel, P. *Atmos. Environ.* **2008**, *42*, 544−553.

(4) Bidleman, T. F.; Billings, W. N.; Foreman, W. T. *Environ. Sci. Technol.* **1986**, *20*, 1038−1043.

(5) Millet, M.; Wortham, H.; Sanusi, A.; Mirabel, P. *Environ. Sci. Pollut. Res.* **1997**, *4*, 172−180.

(6) Atkinson, R. *Gas Phase Tropospheric Chemistry of Organic Compounds*; Royal Society of Chemistry: London, 1995.

(7) Plimmer, J. R.; Johnson, W. *Pesticide Degradation Products in the Atmosphere*; American Chemical Society: Washington, DC, 1991.

(8) WHO Specifications and Evaluations for Public Health Pesticides, Pirimiphos-Methyl, 19.

(9) Siebers, J.; Binner, R.; Wittich, K. P. *Chemosphere* **2003**, *51*, 397−407.

(10) Eneji, I. S.; Buncel, E.; VanLoon, G. W. *J. Agric. Food Chem.* **2002**, *50*, 5634−5639.

(11) Chiron, S.; Rodriguez, A.; Fernandez-Alba, A. *J. Chromatogr., A* **1998**, *823*, 97−107.

(12) Herrmann, J. M.; Guillard, C.; Arguello, M.; Agüera, A.; Tejedor, A.; Piedra, L.; Fernández-Alba, A. *Catal. Today* **1999**, *54*, 353−367.
(13) Hardt, J.; Angerer, J. *J. Chromatogr., B* **1999**, *730*, 229−238.
(14) Chen, T.; Fu, F.; Chen, Z.; Li, D.; Zhang, L.; Chen, G. *J. Chromatogr., A* **2009**, *1216*, 3217−3222.
(15) Pirisi, F. M.; Cabras, P.; Garau, V. L.; Melis, M.; Secchi, E. *J. Agric. Food Chem.* **1996**, *44*, 2417−2422.
(16) Yang, B.; Zhang, Y.; Meng, J.; Gan, J.; Shu, J. *Environ. Sci. Technol.* **2010**, *44*, 3311−3316.
(17) Zhang, Y.; Yang, B.; Meng, J. W.; Gao, S. K.; Dong, X. Y.; Shu, J. I. *Atmos. Environ.* **2010**, *44*, 697−702.
(18) Shu, J.; Gao, S.; Li, Y. *Aerosol Sci. Technol.* **2008**, *42*, 110−113.
(19) Yang, B.; Meng, J.; Zhang, Y.; Liu, C.; Gan, J.; Shu, J. *Atmos. Environ.* **2011**, *45*, 2074−2079.
(20) Finlayson-Pitts, B. J.; Pitts, J. N. *Chemistry of the Upper and Lower Atmosphere: Theory, Experiments, and Applications*; Academic Press: New York, 2000.
(21) Evaluated Kinetic Data. http://www.iupac-kinetic.ch.cam.ac.uk/.
(22) Frisch, M. J.; Trucks, G. W.; Schlegel, H. B.; Scuseria, G. E.; Robb, M. A.; Cheeseman, J. R.; Scalmani, G.; Barone, V.; Mennucci, B.; Petersson, G. A.; et al. *Gaussian 09*, revision A.02; Gaussian, Inc.: Wallingford CT, 2009.
(23) Ide, T.; Nakayama, T.; Takahashi, K.; Matsumi, Y. *Int. J. Chem. Kinet.* **2008**, *40*, 679−684.
(24) Gross, S.; Bertram, A. K. *J. Phys. Chem. A* **2008**, *112*, 3104−3113.
(25) Knopf, D. A.; Forrester, S. M.; Slade, J. H. *Phys. Chem. Chem. Phys.* **2011**, *13*, 21050−21062.
(26) Gross, S.; Iannone, R.; Xiao, S.; Bertram, A. K. *Phys. Chem. Chem. Phys.* **2009**, *11*, 7792−7803.
(27) Atkinson, R.; Arey, J. *Environ. Health Perspect.* **1994**, *102*, 117−126.
(28) Vereecken, L. *Chem. Phys. Lett.* **2008**, *466*, 127−130.
(29) Donahue, N.; Robinson, A.; Hartz, K. E. H.; Sage, A.; Weitkamp, E. *Geophys. Res. Lett.* **2005**, *32*, L16805.
(30) Liu, C.; Zhang, P.; Yang, B.; Wang, Y.; Shu, J. *Environ. Sci. Technol.* **2012**, *46*, 7575−7580.
(31) Aschmann, S. M.; Atkinson, R. *J. Phys. Chem. A* **2006**, *110*, 13029−13035.
(32) Thornberry, T.; Abbatt, J. *Phys. Chem. Chem. Phys.* **2004**, *6*, 84−93.
(33) Perraudin, E.; Budzinski, H.; Villenave, E. *J. Atmos. Chem.* **2007**, *56*, 57−82.
(34) Mmereki, B. T.; Donaldson, D. *J. Phys. Chem. A* **2003**, *107*, 11038−11042.
(35) Atkinson, R. *J. Phys. Chem. Ref. Data* **1991**, *20*, 459−507.
(36) Shu, Y.; Atkinson, R. *J. Geophys. Res.* **1995**, *100*, 7275−7281.
(37) Sasaki, J.; Aschmann, S. M.; Kwok, E. S. C.; Atkinson, R.; Arey, J. *Environ. Sci. Technol.* **1997**, *31*, 3173−3179.
(38) Nakatsugawa, T.; Dahm, P. A. *Biochem. Pharmacol.* **1967**, *16*, 25−38.